Numerical Simulation of Coastal Flows in Open Multiply-Connected Irregular Domains

Yuri N. Skiba[1] and Denis M. Filatov[2]

[1] Centre for Atmospheric Sciences (CCA),
National Autonomous University of Mexico (UNAM),
Av. Universidad 3000, C.P. 04510, Mexico City, Mexico
[2] Centre for Computing Research (CIC), National Polytechnic Institute (IPN),
Av. Juan de Dios Batiz s/n, C.P. 07738, Mexico City, Mexico
skiba@unam.mx, denisfilatov@gmail.com

Abstract. We develop a numerical method for the simulation of coastal flows in multiply-connected domains with irregular boundaries that may contain both closed and open segments. The governing equations are the shallow-water model. Our method involves splitting of the original nonlinear operator by physical processes and by coordinates. Specially constructed finite-difference approximations provide second-order unconditionally stable schemes that conserve the mass and the total energy of the discrete inviscid unforced shallow-water system, while the potential enstrophy results to be bounded, oscillating in time within a narrow range. This allows numerical simulation of coastal flows adequate both from the mathematical and physical standpoints. Several numerical experiments, including those with complex boundaries, demonstrate the skilfulness of the method.

Keywords: Coastal Shallow-water Flows, Conservative Finite Difference Schemes, Multiply-connected Domains, Irregular Boundaries, Operator Splitting.

1 Introduction

When studying a 3D fluid dynamics problem in which typical horizontal scales are much larger than the vertical ones—say, the vertical component of the velocity field is rather small compared to the horizontal ones, or horizontal movements of the fluid are normally much larger than the vertical ones—it is often useful to reduce the original problem, usually described by the Navier-Stokes equations, to a 2D approximation. This leads to a shallow-water model [19, 10, 6].

Shallow-water equations (SWEs) naturally arise in the researches of global atmospheric circulation, tidal waves, river flows, tsunamis, among others [5]. In the spherical coordinates (λ, φ) the shallow-water equations for an ideal unforced fluid can be written as [18]

$$\frac{\partial U}{\partial t} + \frac{1}{R\cos\varphi}\frac{1}{2}\left[\left(\frac{\partial uU}{\partial \lambda} + u\frac{\partial U}{\partial \lambda}\right) + \left(\frac{\partial vU\cos\varphi}{\partial \varphi} + v\cos\varphi\frac{\partial U}{\partial \varphi}\right)\right] - \left(f + \frac{u}{R}\tan\varphi\right)V = -\frac{gz}{R\cos\varphi}\frac{\partial h}{\partial \lambda}, \quad (1)$$

M.S. Obaidat et al. (eds.), *Simulation and Modeling Methodologies, Technologies and Applications*, Advances in Intelligent Systems and Computing 256,
DOI: 10.1007/978-3-319-03581-9_5,

$$\frac{\partial V}{\partial t}+\frac{1}{R\cos\varphi}\frac{1}{2}\left[\left(\frac{\partial uV}{\partial\lambda}+u\frac{\partial V}{\partial\lambda}\right)+\left(\frac{\partial vV\cos\varphi}{\partial\varphi}+v\cos\varphi\frac{\partial V}{\partial\varphi}\right)\right]$$
$$+\left(f+\frac{u}{R}\tan\varphi\right)U=-\frac{gz}{R}\frac{\partial h}{\partial\varphi}, \tag{2}$$
$$\frac{\partial h}{\partial t}+\frac{1}{R\cos\varphi}\left[\frac{\partial zU}{\partial\lambda}+\frac{\partial zV\cos\varphi}{\partial\varphi}\right]=0. \tag{3}$$

Here $U\equiv uz$, $V\equiv vz$, where $u=u(\lambda,\varphi,t)$ and $v=v(\lambda,\varphi,t)$ are the fluid's velocity components, $H=H(\lambda,\varphi,t)$ is the fluid's depth, $z\equiv\sqrt{H}$, $f=f(\varphi)$ is the Coriolis acceleration due to the rotation of the sphere, R is the radius of the sphere, $h=h(\lambda,\varphi,t)$ is the free surface height, g is the gravitational acceleration. Besides, $h=H+h_T$, where $h_T=h_T(\lambda,\varphi)$ is the bottom topography. We shall study (1)-(3) in a bounded domain D on a sphere with an arbitrary piecewise smooth boundary Γ, assuming that λ is the longitude (positive eastward) and φ is the latitude (positive northward).

As we are dealing with a boundary value problem, system (1)-(3) has to be equipped with boundary conditions.

The question of imposing correct boundary conditions for SWEs is not trivial. Many independent research papers have been dedicated to this issue for the last several decades [19, 9, 20, 1]. Depending on the type of the boundary—inflow, outflow or closed—as well as on the particular physical application, one or another set of boundary conditions should be used. Following [1], we represent the boundary as $\Gamma=\Gamma_{\rm o}\cup\Gamma_{\rm c}$, where $\Gamma_{\rm o}$ is the open part of the boundary, while $\Gamma_{\rm c}$ is its closed part. Such a representation of the boundary simulates a bay-like domain, where the coastline corresponds to the closed part $\Gamma_{\rm c}$, while the influence of the ocean is modelled via the open segment $\Gamma_{\rm o}$. Yet, the open segment is divided into the inflow $\Gamma_{\rm inf}:=\{(\lambda,\varphi)\in\Gamma:\mathbf{n}\cdot\mathbf{u}<0\}$ and outflow $\Gamma_{\rm out}:=\{(\lambda,\varphi)\in\Gamma:\mathbf{n}\cdot\mathbf{u}>0\}$. Here $\mathbf{n}$ is the outward unit normal to Γ, $\mathbf{u}=(u,v)^{\rm T}$. On the closed part we put

$$\mathbf{n}\cdot\mathbf{u}=0, \tag{4}$$

on the inflow we assume

$$\tau\cdot\mathbf{u}=0,\qquad h=h_{(\Gamma)} \tag{5}$$

and on the outflow it holds

$$h=h_{(\Gamma)}, \tag{6}$$

where τ is the tangent vector to Γ, whereas $h_{(\Gamma)}$ is a given function defined on the boundary [1].

From the mathematical standpoint unforced inviscid SWEs are based on several conservation laws. In particular, the mass

$$M(t)=\int_D HdD, \tag{7}$$

the total energy

$$E(t) = \frac{1}{2} \int_D \left[\left(u^2 + v^2\right) H + g \left(h^2 - h_T^2\right) \right] dD \tag{8}$$

and the potential enstrophy

$$J(t) = \frac{1}{2} \int_D H \left(\frac{\zeta + f}{H} \right)^2 dD, \tag{9}$$

where

$$\zeta = \frac{1}{R \cos \varphi} \left(\frac{\partial v}{\partial \lambda} - \frac{\partial u \cos \varphi}{\partial \varphi} \right), \tag{10}$$

are kept constant in time for a closed shallow-water system [20, 6]. In the numerical simulation of shallow-water flows one should use the finite difference schemes which preserve the discrete analogues of the integral invariants of motion (7)-(9) as accurately as possible. It is crucial that for many finite difference schemes the discrete analogues of the mass, total energy and potential enstrophy are usually not invariant in time, so the numerical method can be unstable and the resulting simulation becomes inaccurate [20]. This emphasises the importance of using conservative difference schemes while modelling fluid dynamics phenomena.

In the last forty years there have been suggested several finite difference schemes that conserve some or other integral characteristics of the shallow-water equations [12, 2, 4, 11, 3, 7, 13]. In all these works, however, only semi–discrete (i.e., discrete only in space, but still continuous in time) conservative schemes are constructed. After using an explicit time discretisation those schemes stop being conservative. Besides, while aiming to achieve the desired full conservatism (see, e.g., [14]), when all the discrete analogues of the integral invariants of motion are conserved, some methods require rather complicated spatial grids (e.g., triangular, hexagonal, etc.), which makes it difficult to employ those methods in a computational domain with a boundary of an arbitrary shape; alternatively, it may result in a resource-intensive numerical algorithm.

In this work we suggest a new efficient method for the numerical simulation of shallow-water flows in domains of complex geometries. The method is based on our earlier research devoted to the modelling of atmospheric waves with SWEs [16–18]. The method involves operator splitting of the original equations by physical processes and by coordinates. Careful subsequent discretisation of the split 1D systems coupled with the Crank-Nicolson approximation of the spatial terms yields a fully discrete (i.e., discrete both in time and in space) finite difference shallow-water model that, in case of an inviscid and unforced fluid, exactly conserves the mass and the total energy, while the potential enstrophy is bounded, oscillating in time within a narrow band. Due to the prior splitting the model is extremely efficient, since it is implemented as systems of linear algebraic equations with tri– and five–diagonal matrices. Furthermore, the model can straightforwardly be realised on high-performance parallel computers without any significant modifications in the original single-threaded algorithm.

The paper is organised as follows. In Section 2 we give the mathematical foundations of the suggested shallow-water model. In Section 3 we test the model with several

numerical experiments aimed to simulate shallow-water flows in a bay-like domain with a complex boundary. We also test a modified model, taking into account fluid viscosity and external forcing for providing more realistic simulation. In Section 4 we give a conclusion.

2 Governing Equations of the Fully Discrete Conservative Shallow-Water Model

Rewrite the shallow-water equations (1)-(3) in the operator form

$$\frac{\partial \boldsymbol{\psi}}{\partial t} + \mathbf{A}(\boldsymbol{\psi}) = 0, \tag{11}$$

where $\mathbf{A}(\boldsymbol{\psi})$ is the shallow-water nonlinear operator, while $\boldsymbol{\psi} = (U, V, h\sqrt{g})^{\mathrm{T}}$ is the unknown vector. Now represent the operator $\mathbf{A}(\boldsymbol{\psi})$ as a sum of three simpler operators, nonlinear $\mathbf{A_1}$, $\mathbf{A_2}$ and linear $\mathbf{A_3}$

$$\mathbf{A}(\boldsymbol{\psi}) = \mathbf{A_1}(\boldsymbol{\psi}) + \mathbf{A_2}(\boldsymbol{\psi}) + \mathbf{A_3}\boldsymbol{\psi}. \tag{12}$$

Let (t_n, t_{n+1}) be a sufficiently small time interval with a step τ ($t_{n+1} = t_n + \tau$). Applying in (t_n, t_{n+1}) operator splitting to (11), we approximate it by the three simpler problems

$$\frac{\partial \boldsymbol{\psi}_1}{\partial t} + \mathbf{A_1}(\boldsymbol{\psi}_1) = 0, \tag{13}$$

$$\frac{\partial \boldsymbol{\psi}_2}{\partial t} + \mathbf{A_2}(\boldsymbol{\psi}_2) = 0, \tag{14}$$

$$\frac{\partial \boldsymbol{\psi}_3}{\partial t} + \mathbf{A_3}\boldsymbol{\psi}_3 = 0. \tag{15}$$

According to the method of splitting, these problems are to be solved one after another, so that the solution to (11) from the previous time interval (t_{n-1}, t_n) is the initial condition for (13): $\boldsymbol{\psi}_1(t_n) = \boldsymbol{\psi}(t_n)$, then $\boldsymbol{\psi}_2(t_n) = \boldsymbol{\psi}_1(t_{n+1})$ and finally $\boldsymbol{\psi}_3(t_n) = \boldsymbol{\psi}_2(t_{n+1})$. Therefore, the solution to (11) at the moment t_{n+1} is approximated by the solution $\boldsymbol{\psi}_3(t_{n+1})$ [8].

Operators $\mathbf{A_1}$, $\mathbf{A_2}$, $\mathbf{A_3}$ can be defined in different ways. In our work equation (13) has the form

$$\frac{\partial U}{\partial t} + \frac{1}{R\cos\varphi}\frac{1}{2}\left[\frac{\partial uU}{\partial \lambda} + u\frac{\partial U}{\partial \lambda}\right] = -\frac{gz}{R\cos\varphi}\frac{\partial h}{\partial \lambda}, \tag{16}$$

$$\frac{\partial V}{\partial t} + \frac{1}{R\cos\varphi}\frac{1}{2}\left[\frac{\partial uV}{\partial \lambda} + u\frac{\partial V}{\partial \lambda}\right] = 0, \tag{17}$$

$$\frac{\partial h}{\partial t} + \frac{1}{R\cos\varphi}\frac{\partial zU}{\partial \lambda} = 0, \tag{18}$$

for (14) we take

$$\frac{\partial U}{\partial t} + \frac{1}{R\cos\varphi}\frac{1}{2}\left[\frac{\partial vU\cos\varphi}{\partial \varphi} + v\cos\varphi\frac{\partial U}{\partial \varphi}\right] = 0, \tag{19}$$

$$\frac{\partial V}{\partial t}+\frac{1}{R\cos\varphi}\frac{1}{2}\left[\frac{\partial vV\cos\varphi}{\partial\varphi}+v\cos\varphi\frac{\partial V}{\partial\varphi}\right]=-\frac{gz}{R}\frac{\partial h}{\partial\varphi}, \tag{20}$$

$$\frac{\partial h}{\partial t}+\frac{\partial zV\cos\varphi}{\partial\varphi}=0, \tag{21}$$

and for (15)—

$$\frac{\partial U}{\partial t}-\left(f+\frac{u}{R}\tan\varphi\right)V=0, \tag{22}$$

$$\frac{\partial V}{\partial t}+\left(f+\frac{u}{R}\tan\varphi\right)U=0. \tag{23}$$

This choice of $\mathbf{A_i}$'s corresponds to the splitting by physical processes (transport and rotation) and by coordinates (λ and φ). The latter means that while solving (16)-(18) in λ, the coordinate φ is left fixed; and vice versa for (19)-(21).

Introducing the grid $\{(\lambda_k,\varphi_l)\in D:\lambda_{k+1}=\lambda_k+\Delta\lambda,\varphi_{l+1}=\varphi_l+\Delta\varphi\}$, we approximate systems (16)-(18) and (19)-(21) by the central second-order finite difference schemes, so that eventually in λ we obtain (the subindex l, in the φ–direction, is fixed, as well as omitted for simplicity)

$$\frac{U_k^{n+1}-U_k^n}{\tau}+\frac{1}{2c_l}\left[\frac{\overline{u}_{k+1}U_{k+1}-\overline{u}_{k-1}U_{k-1}}{2\Delta\lambda}+\overline{u}_k\frac{U_{k+1}-U_{k-1}}{2\Delta\lambda}\right]$$
$$=-\frac{g\overline{z}_k}{c_l}\frac{h_{k+1}-h_{k-1}}{2\Delta\lambda}, \tag{24}$$

$$\frac{V_k^{n+1}-V_k^n}{\tau}+\frac{1}{2c_l}\left[\frac{\overline{u}_{k+1}V_{k+1}-\overline{u}_{k-1}V_{k-1}}{2\Delta\lambda}+\overline{u}_k\frac{V_{k+1}-V_{k-1}}{2\Delta\lambda}\right]=0, \tag{25}$$

$$\frac{h_k^{n+1}-h_k^n}{\tau}+\frac{1}{c_l}\frac{\overline{z}_{k+1}U_{k+1}-\overline{z}_{k-1}U_{k-1}}{2\Delta\lambda}=0, \tag{26}$$

while in φ we get (the subindex k, in λ, is fixed and omitted too)

$$\frac{U_l^{n+1}-U_l^n}{\tau}+\frac{1}{2c_l}\left[\frac{\overline{v}_{l+1}U_{l+1}c_+-\overline{v}_{l-1}U_{l-1}c_-}{2\Delta\varphi}+\overline{v}_l\cos\varphi_l\frac{U_{l+1}-U_{l-1}}{2\Delta\varphi}\right]=0, \tag{27}$$

$$\frac{V_l^{n+1}-V_l^n}{\tau}+\frac{1}{2c_l}\left[\frac{\overline{v}_{l+1}V_{l+1}c_+-\overline{v}_{l-1}V_{l-1}c_-}{2\Delta\varphi}+\overline{v}_l\cos\varphi_l\frac{V_{l+1}-V_{l-1}}{2\Delta\varphi}\right]$$
$$=-\frac{g\overline{z}_l}{R}\frac{h_{l+1}-h_{l-1}}{2\Delta\varphi}, \tag{28}$$

$$\frac{h_l^{n+1}-h_l^n}{\tau}+\frac{1}{c_l}\frac{\overline{z}_{l+1}V_{l+1}c_+-\overline{z}_{l-1}V_{l-1}c_-}{2\Delta\varphi}=0. \tag{29}$$

Here, in a standard manner, $w_{kl}^n=w(\lambda_k,\varphi_l,t_n)$, where $w=\{U,V,h\}$; besides, we denoted $c_l\equiv R\cos\varphi_l$ and $c_\pm\equiv\cos\varphi_{l\pm1}$. In turn, the rotation problem (22)-(23) has the form

$$\frac{U_{kl}^{n+1}-U_{kl}^n}{\tau}-\left(f_l+\frac{\overline{u}_{kl}}{R}\tan\varphi_l\right)V_{kl}=0, \tag{30}$$

$$\frac{V_{kl}^{n+1}-V_{kl}^n}{\tau}+\left(f_l+\frac{\overline{u}_{kl}}{R}\tan\varphi_l\right)U_{kl}=0. \tag{31}$$

The functions U_{kl}, V_{kl} in the presented schemes are defined via the Crank-Nicolson approximation as $U_{kl} = \left(U_{kl}^n + U_{kl}^{n+1}\right)/2$, $V_{kl} = \left(V_{kl}^n + V_{kl}^{n+1}\right)/2$. As for the overlined functions $\overline{u}_{kl}$, $\overline{v}_{kl}$ and $\overline{z}_{kl}$, they can be chosen in an arbitrary manner [16]. For instance, the choice $\overline{w}_{kl} = w_{kl}^n$, where $w = \{u, v, z\}$, will yield linear second-order finite difference schemes, whereas the choice $\overline{w}_{kl} = w_{kl}$ coupled with the corresponding Crank-Nicolson approximations for w_{kl} will produce nonlinear schemes.

The developed schemes have several essential advantages.

First, the coordinate splitting allows simple parallelisation of the numerical algorithm without any significant modifications of the single-threaded code. Indeed, say, when solving (24)-(26), all the calculations along the longitude at different φ_l's can be done in parallel; analogously, for (27)-(29) the calculations at different λ_k's are naturally parallelisable. Finally, equations (30)-(31) can be reduced to explicit formulas with respect to U_{kl}^{n+1}, V_{kl}^{n+1} [17].

Second, the simple 1D longitudinal and latitudinal spatial stencils used do not impose any restrictions on the shape of the boundary Γ. Therefore, the developed schemes can be employed for the simulation of shallow-water flows in computational domains of complex geometries.

Third, the developed schemes are mass– and total-energy–conserving for the inviscid unforced shallow-water model in a closed basin ($\Gamma = \Gamma_c$). To show this, consider, e.g., (24)-(26). The boundary condition will be $U|_\Gamma = 0$, which can be approximated as

$$\frac{1}{2}\left(U_0 + U_1\right) = 0, \tag{32}$$

$$\frac{1}{2}\left(U_K + U_{K+1}\right) = 0, \tag{33}$$

where the nodes $k = 1$ and $k = K$ are inside the domain D, while the nodes $k = 0$ and $k = K + 1$ are out of D (i.e., fictitious). Multiplying (26) by $\tau R \Delta\lambda$, summing over all the $k = \overline{1, K}$'s and taking into account the boundary conditions (32)-(33), we find that the spatial term vanishes, so that

$$M_l^{n+1} = R\Delta\lambda \sum_k H_{kl}^{n+1} = \cdots = R\Delta\lambda \sum_k H_{kl}^n = M_l^n, \tag{34}$$

which proves that the mass conserves in λ (at a fixed l). Further, multiplying (24) by $\tau R \Delta\lambda U_{kl}$, (25) by $\tau R \Delta\lambda V_{kl}$ and (26) by $\tau R \Delta\lambda g h_{kl}$, summing over the internal k's and taking into account (32)-(33), we obtain

$$\begin{aligned} E_l^{n+1} &= R\Delta\lambda \sum_k \frac{1}{2}\left(\left[U_{kl}^{n+1}\right]^2 + \left[V_{kl}^{n+1}\right]^2 + g\left(\left[h_{kl}^{n+1}\right]^2 - \left[h_{T,kl}\right]^2\right)\right) = \cdots \\ &= R\Delta\lambda \sum_k \frac{1}{2}\left(\left[U_{kl}^{n}\right]^2 + \left[V_{kl}^{n}\right]^2 + g\left(\left[h_{kl}^{n}\right]^2 - \left[h_{T,kl}\right]^2\right)\right) = E_l^n, \end{aligned} \tag{35}$$

that is the energy conserves in λ at $\varphi = \varphi_l$ too. Similar results can be obtained with respect to the second coordinate, φ (problem (27)-(29)), while the Coriolis problem (30)-(31) does not affect the conservation laws. Note that to establish both the mass and the energy conservation we used the divergence of the spatial terms in (24)-(26)

and (27)-(29) [14]. The conservation of the total energy guarantees that the constructed finite difference schemes are absolutely stable [8].

Fourth, from (24)-(26), (27)-(29) it follows that under the choice $\overline{w}_{kl} = w^n_{kl}$, where $w = \{u, v, z\}$, the resulting finite difference schemes are systems of linear algebraic equations with either tri– or five–diagonal matrices. Obviously, fast direct (i.e., non-iterative) linear solvers can be used for their solution, so that the exact conservation of the mass and the total energy will not be violated.

3 Numerical Experiments

For testing the developed model we consider two problems. In the first problem the SWEs are a closed system, so that we are able to verify the mass and the total energy conservation laws; besides, the ranges of the variation of the potential enstrophy are analysed. In the second experiment the problem is complicated by introducing a complex boundary with open and closed segments, a nonzero viscosity, as well as a nonzero source function imitating the wind. Such a setup simulates wind-driven shallow-water flows in a bay.

3.1 Rectangular Domain Test

In this experiment we consider the simplest case: for the computational domain we take the spherical rectangle $D = \{(\lambda, \varphi) : \lambda \in (12.10, 12.65), \varphi \in (45.16, 45.60)\}$ with a closed boundary $\Gamma = \Gamma_c$. This will allow to verify whether the mass and the total energy of an inviscid unforced fluid are exactly conserved in the numerical simulation. For the initial velocity field we take $u = v = 0$, while the free surface height is a hat-like function (Fig. 1). The gridsteps are $\Delta\lambda \approx \Delta\varphi \approx 0.015^\circ$, $\tau = 1.44$ min.

In Fig. 2 we plot a graph of the discrete analogues of the potential enstrophy (9). The mass and the total energy are not shown, as they are trivial constants, that is those invariants are conserved exacly, while the behaviour of the potential enstrophy is stable—it is oscillating within a narrow band, with a drastically small maximum relative error about 0.32%, without unbounded growth or decay. This confirms the theoretical calculations (34)-(35), as well as demonstrates that the developed schemes allow obtaining physically adequate simulation results.

3.2 Irregular Domain Test

Having a numerical shallow-water model that conserves the mass and the total energy in the absence of sources and sinks of energy, now consider a more complex problem.

For the computational domain we choose the region shown in Fig. 3. Unlike the previous problem, the boundary is now of an arbitrary shape; besides, there are several onshore parts surrounded by water which represent small isles. The boundary Γ is divided into the closed and open segments: $\Gamma_o = \{\lambda \in (12.32, 12.65), \varphi = 45.16\} \cup \{\lambda = 12.65, \varphi \in (45.16, 45.50)\}$, $\Gamma_c = \Gamma \backslash \Gamma_o$. This setup aims to simulate flows that may occur in the Bay of Venice.

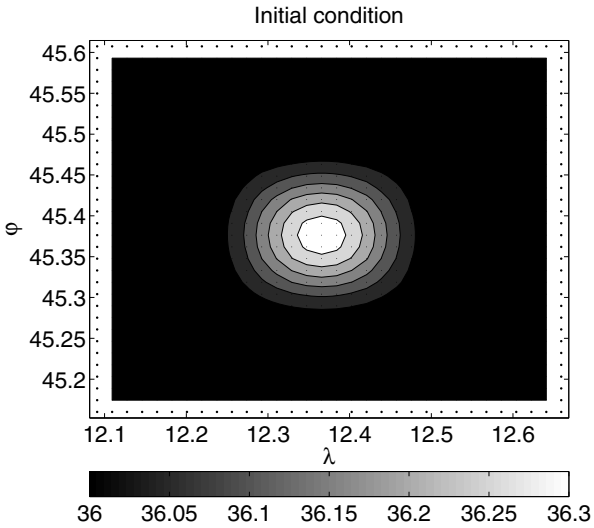

Fig. 1. Rectangular Domain Test: Initial condition (the free surface height is shown in meters; the markers '.' denote the fictitious nodes outside the domain)

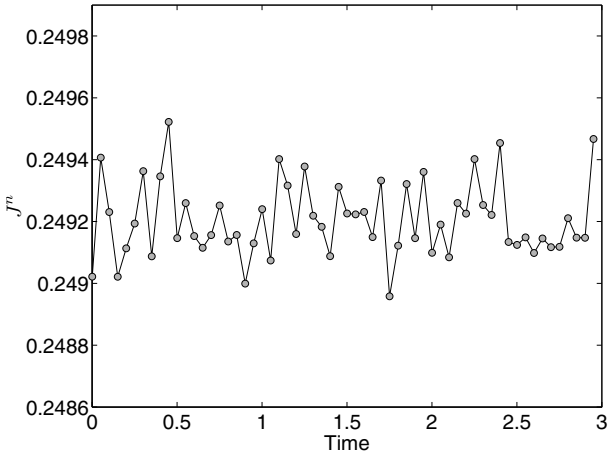

Fig. 2. Rectangular Domain Test: Behaviour of the potential enstrophy in time (in days). Maximum relative error does not exceed 0.32%.

In order to make the flows more realistic, terms responsible for fluid viscosity are also added into the first two equations of the shallow-water system. Specifically, on the right-hand side of (11) we add the vector $\mathbf{D}\boldsymbol{\psi}$, where

$$\mathbf{D} = \begin{pmatrix} d_{11} & 0 & 0 \\ 0 & d_{22} & 0 \\ 0 & 0 & 0 \end{pmatrix}, \tag{36}$$

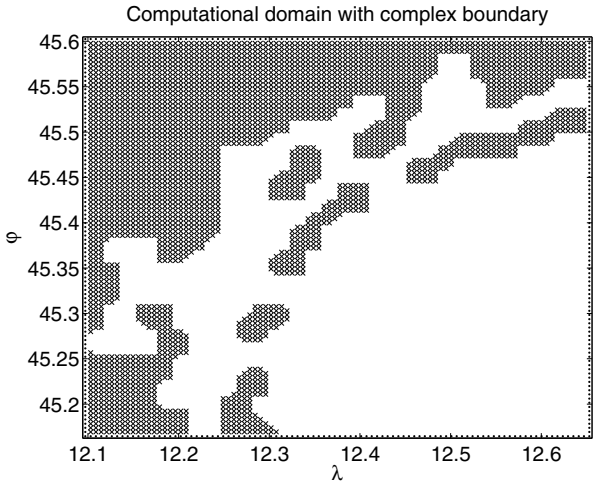

Fig. 3. Irregular Domain Test: The computational domain (white area) with onshore parts and interior isles (grey areas)

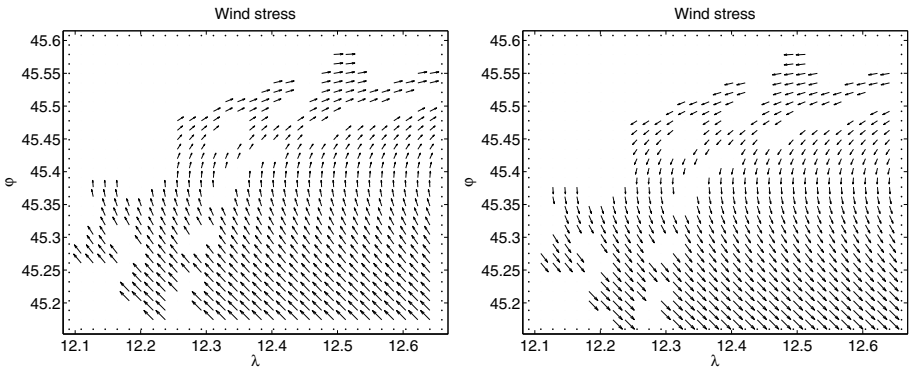

Fig. 4. Irregular Domain Test: Field of the wind stress at $t = 0.25$ (left) and $t = 0.75$ (right)

where

$$d_{11} = d_{22} = \frac{D}{R^2 \cos^2 \varphi} \frac{\partial^2}{\partial \lambda^2} + \frac{D}{R^2 \cos \varphi} \frac{\partial}{\partial \varphi} \left(\cos \varphi \frac{\partial}{\partial \varphi} \right). \tag{37}$$

Here D is the viscosity coefficient. However, addition of the viscosity terms into (24)-(25) and (27)-(28) requires a modification of boundary conditions (4)-(6). Following [1], we use the boundary conditions

$$\mathbf{n} \cdot \mathbf{u} = 0, \qquad Dh \frac{\partial \mathbf{u}}{\partial \mathbf{n}} \tau = 0, \tag{38}$$

$$\left(|\mathbf{n} \cdot \mathbf{u}| - \mathbf{n} \cdot \mathbf{u} \right) \left(h - h_{(\Gamma)} \right) = 0, \tag{39}$$

$$Dh \frac{\partial \mathbf{u}}{\partial \mathbf{n}} = 0. \tag{40}$$

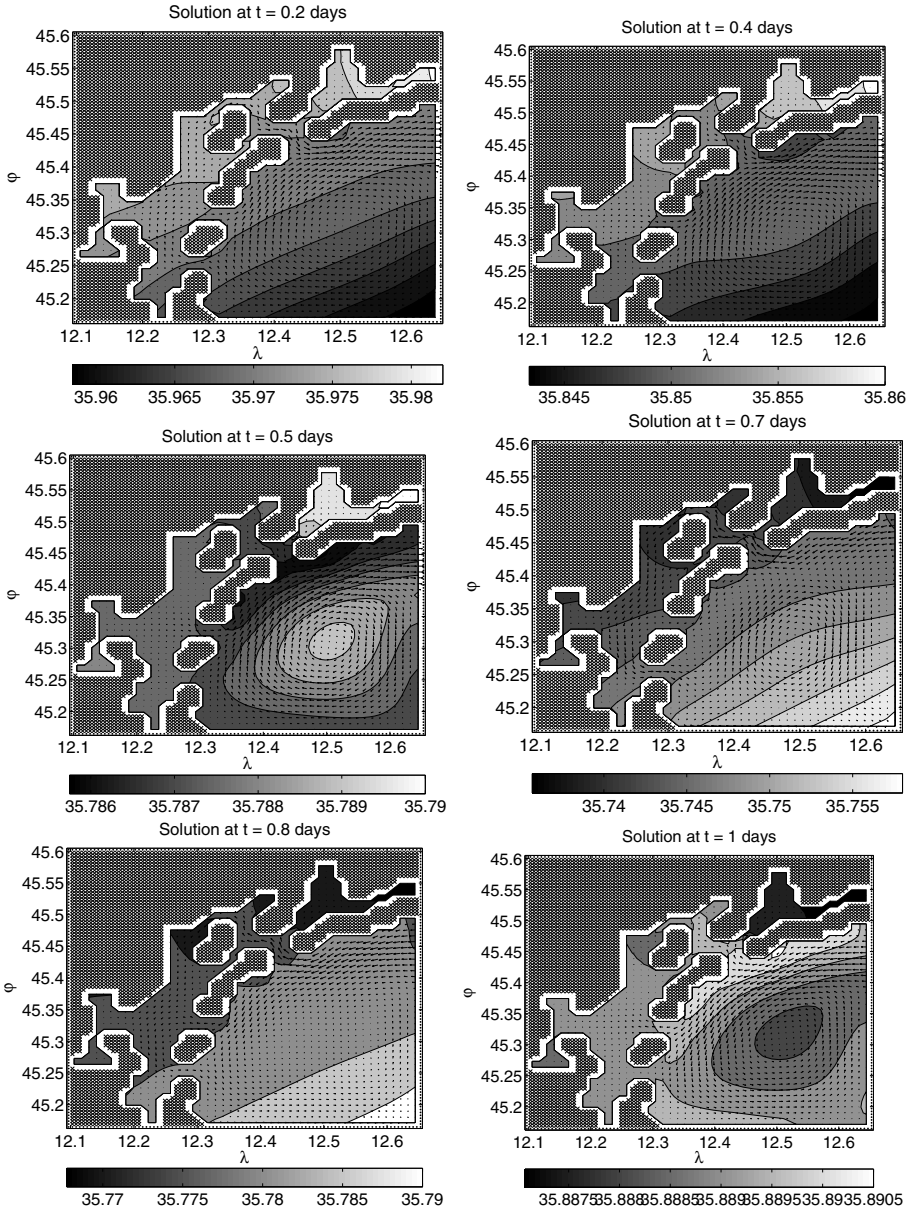

Fig. 5. Irregular Domain Test: Numerical solution at several time moments (the solution is reduced to a coarser grid $\Delta\lambda \approx \Delta\varphi \approx 0.01^\circ$ for better visualisation; the fluid's depth is shown by colour, while the velocity field is shown by arrows)

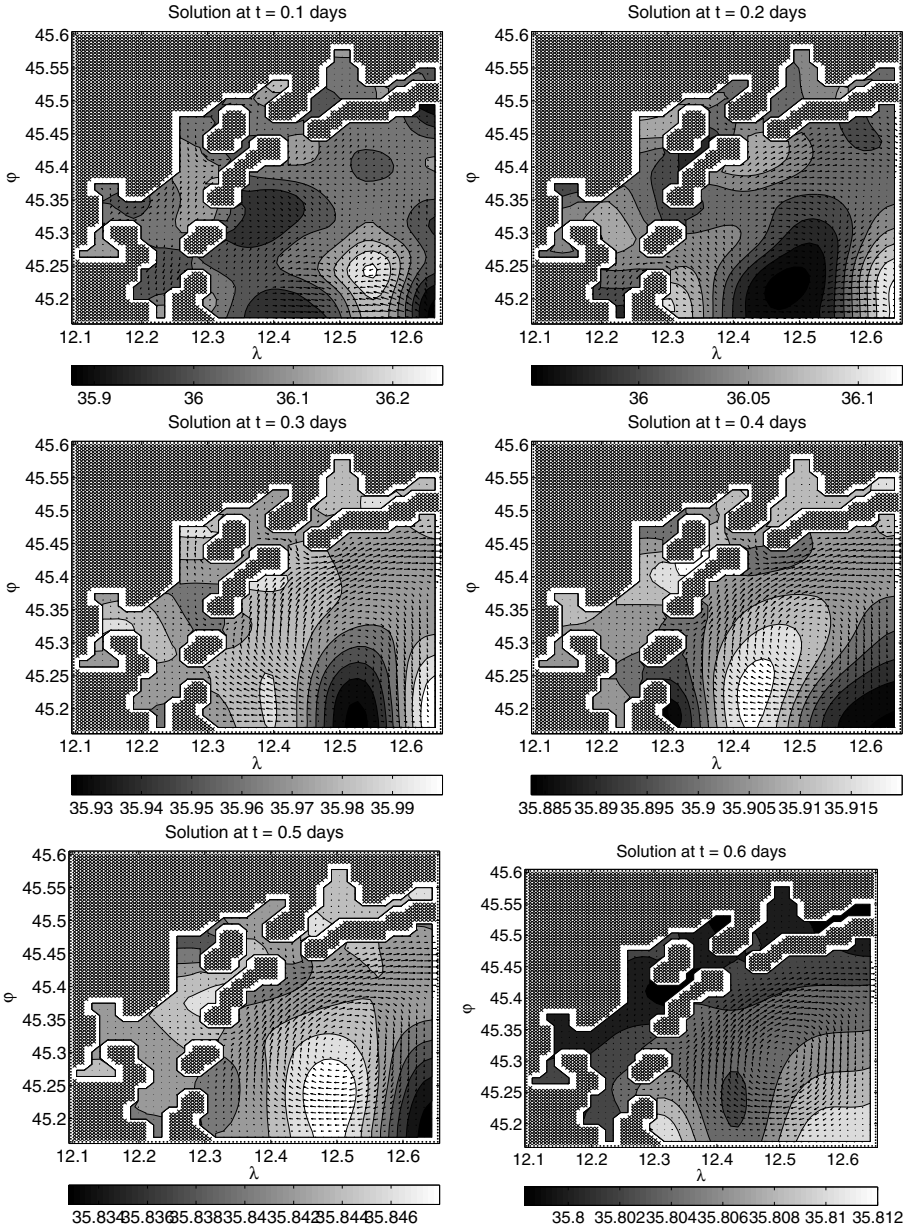

Fig. 6. Irregular Domain Test with Nonzero Bottom Topography: Numerical solution at several time moments

Condition (38) is for $\mathbf{u}$ on the closed segment of the boundary (see also [15]), while (39) and (40) are for h and $\mathbf{u}$ on the open segment, respectively. Condition (39) is supposed to consist of two parts: the first term fires on the outflow (when $|\mathbf{n}\cdot\mathbf{u}| = \mathbf{n}\cdot\mathbf{u}$), whereas the second term is responsible for the inflow ($h_{(\Gamma)}$ is supposed to be given a priori).

Finally, on the right-hand side of (11) we add a wind stress of the form $\mathbf{W}\boldsymbol{\psi}\sin 2\pi t$, where

$$\mathbf{W} \sim \begin{pmatrix} -\cos\frac{\pi(\varphi-\varphi_{\min})}{L_\varphi} & 0 & 0 \\ 0 & \cos\frac{\pi(\varphi-\varphi_{\min})}{2L_\varphi} & 0 \\ 0 & 0 & 0 \end{pmatrix}, \tag{41}$$

while $L_\varphi = \varphi_{\max} - \varphi_{\min}$. The wind stress field at $t = 0.25$ and $t = 0.75$ is shown in Fig. 4.

The numerical solution computed on the grid $\Delta\lambda \approx \Delta\varphi \approx 0.005^\circ$ and $\tau = 1.44$ min is presented in Fig. 5 at several time moments. Comparison with Fig. 4 shows that a wind-driven flow occurs and is then developing in the computational domain. Specifically, as the simulation starts, the velocity field is formed clockwise (Fig. 5, $t = 0.2, 0.4$), in accordance with the wind stress at small times (Fig. 4, left). Later, at $t = 0.5$, the wind's direction changes to anticlockwise due to the term $\sin 2\pi t$, which is reflected in the numerical solution with a little time gap because of the fluid's inertia, especially in the open ocean far from the coastline: while the coastal waters change their flows at $t \approx 0.5 - 0.7$, the large vortex in the open bay begins rotating anticlockwise at $t \approx 0.8$ (Fig. 5). Finally, at $t = 1$ the entire velocity field is aligned in accordance with the late-time wind stress (Fig. 4, right).

In Fig. 6 we show the numerical solution to a slightly complicated problem—the bottom topography is now a smooth hat-like function with the epicentre at $\lambda_c = 12.51$, $\varphi_c = 45.24$. The diameter of the bottom's irregularity is about 0.1°, maximum height is about 1.6 m. As it is seen from the figure, unlike the previous case the presence of an underwater obstacle causes permutations in the depth field around, while the structure of the velocity field keeps mostly unchanged in time (cf. Fig. 5).

4 Conclusions

A new fully discrete mass– and total-energy–conserving finite difference model for the simulation of shallow-water flows in bay-like domains with complex boundaries was developed. Having taken the SWEs written in the divergent form, we involved the idea of operator splitting coupled with the Crank-Nicolson approximation and constructed absolutely stable second-order finite difference schemes that allow accurate simulation of shallow-water flows in spherical domains of arbitrary shapes. An important integral invariant of motion of the SWEs, the potential enstrophy, proved to be bounded for an inviscid unforced fluid, oscillating in time within a narrow range. Hence, the numerical solution is mathematically accurate and provides physically adequate results. Due to the method of splitting the developed model can straightforwardly be implemented for distributed simulation of shallow-water flows on high-performance parallel computers. Numerical experiments with a simple inviscid unforced closed shallow-water

system and with a viscous open wind-driven shallow-water model with zero and nonzero bottom topography, simulating real situations, nicely confirmed the skills of the new method.

Acknowledgements. This work was supported by Mexican System of Researchers (SNI) grants 14539 and 26073. It is part of the project PAPIIT DGAPA UNAM IN104811-3.

References

1. Agoshkov, V.I., Saleri, F.: Recent Developments in the Numerical Simulation of Shallow Water Equations. Part III: Boundary Conditions and Finite Element Approximations in the River Flow Calculations. Math. Modelling 8, 3–24 (1996)
2. Arakawa, A., Lamb, V.R.: A Potential Enstrophy and Energy Conserving Scheme for the Shallow-Water Equation. Mon. Wea. Rev. 109, 18–36 (1981)
3. Bouchut, F., Le Sommer, J., Zeitlin, V.: Frontal Geostrophic Adjustment and Nonlinear Wave Phenomena in One-dimensional Rotating Shallow Water. Part II: High-Resolution Numerical Simulations. J. Fluid Mech. 514, 35–63 (2004)
4. Heikes, R., Randall, D.A.: Numerical Integration of the Shallow-Water Equations on a Twisted Icosahedral Grid. Part I: Basic Design and Results of Tests. Mon. Wea. Rev. 123, 1862–1880 (1995)
5. Jirka, G.H., Uijttewaal, W.S.J.: Shallow Flows. Taylor & Francis, London (2004)
6. Kundu, P.K., Cohen, I.M., Dowling, D.R.: Fluid Mecanics, 5th edn. Academic Press, London (2012)
7. LeVeque, R.J., George, D.L.: High-Resolution Finite Volume Methods for the Shallow-Water Equations with Bathymetry and Dry States. In: Yeh, H., Liu, P.L., Synolakis, C.E. (eds.) Advanced Numerical Models for Simulating Tsunami Waves and Runup, pp. 43–73. World Scientific Publishing, Singapore (2007)
8. Marchuk, G.I.: Methods of Computational Mathematics. Springer, Berlin (1982)
9. Oliger, J., Sündstrom, A.: Theoretical and Practical Aspects of Some Initial Boundary Value Problems in Fluid Dynamics. SIAM J. Appl. Anal. 35, 419–446 (1978)
10. Pedlosky, J.: Geophysical Fluid Dynamics, 2nd edn. Springer (1987)
11. Ringler, T.D., Randall, D.A.: A Potential Enstrophy and Energy Conserving Numerical Scheme for Solution of the Shallow-Water Equations on a Geodesic Grid. Mon. Wea. Rev. 130, 1397–1410 (2002)
12. Sadourny, R.: The Dynamics of Finite-Difference Models of the Shallow-Water Equations. J. Atmos. Sci. 32, 680–689 (1975)
13. Salmon, R.: A Shallow Water Model Conserving Energy and Potential Enstrophy in the Presence of Boundaries. J. Mar. Res. 67, 1–36 (2009)
14. Shokin, Y.I.: Completely Conservative Difference Schemes. In: de Vahl Devis, G., Fletcher, C. (eds.) Computational Fluid Dynamics, pp. 135–155. Elsevier, Amsterdam (1988)
15. Simonnet, E., Ghil, M., Ide, K., Temam, R., Wang, S.: Low-Frequency Variability in Shallow-Water Models of the Wind-Driven Ocean Circulation. Part I: Steady-State Solution. J. Phys. Ocean. 33, 712–728 (2003)
16. Skiba, Y.N.: Total Energy and Mass Conserving Finite Difference Schemes for the Shallow-Water Equations. Russ. Meteorol. Hydrology 2, 35–43 (1995)
17. Skiba, Y.N., Filatov, D.M.: Conservative Arbitrary Order Finite Difference Schemes for Shallow-Water Flows. J. Comput. Appl. Math. 218, 579–591 (2008)

18. Skiba, Y.N., Filatov, D.M.: Simulation of Soliton-like Waves Generated by Topography with Conservative Fully Discrete Shallow-Water Arbitrary-Order Schemes. Internat. J. Numer. Methods Heat Fluid Flow 19, 982–1007 (2009)
19. Vol'tsynger, N.E., Pyaskovskiy, R.V.: The Theory of Shallow Water. Gidrometeoizdat, St. Petersburg (1977)
20. Vreugdenhil, C.B.: Numerical Methods for Shallow-Water Flow. Kluwer Academic, Dordrecht (1994)